Journal of Engineering Mathematics (2024) 148:6
https://doi.org/10.1007/s10665-024-10393-9

Experimental and theoretical investigation of impinging droplet solidification at moderate impact velocities

Ryan McGuan[1] · Elaheh Alizadeh-Birjandi[1] · Peiwen Yan[1] · Stephen H. Davis[2] · H. Pirouz Kavehpour[1]

Received: 23 April 2024 / Accepted: 14 August 2024

Abstract
Spreading of liquid drops on cold solid substrates is a complicated problem that involves heat transfer, fluid dynamics, and phase change physics combined with complex wetting behaviors at the contact line. Understanding the physics behind the non-isothermal spreading of droplet is of utmost importance due to its broad applications in diverse areas of industry such as in additive manufacturing processes. This work mainly focuses on determining the important physical parameters involved in the non-isothermal spreading of droplets with low contact angle ($\theta < \pi/2$) as well as controlling the post-solidification geometry of impinging droplets with moderate impact velocity where spreading is driven by impact velocities, but fingerings or instabilities do not occur at the contact line. Using analytical modeling, a possible explanation for contact-line arrest is produced that demonstrates that the final radius of droplets of moderate impacting velocity is independent of the initial conditions including the impact dynamics and temperature gradients. The predictive capacity of this model is confirmed with experimental results.

Keywords Solidification · Impact · Spreading · Drops

✉ Peiwen Yan
peteryan966@g.ucla.edu

✉ H. Pirouz Kavehpour
pirouz@seas.ucla.edu

[1] Department of Mechanical and Aerospace Engineering, University of California, Los Angeles, CA 90095, USA

[2] Department of Engineering Sciences and Applied Mathematics, Northwestern University, Evanston, IL 60208, USA

Published online: 04 September 2024

1 Introduction

Three-dimensional (3D) printing technology has been around since the 1980s. This technology is able to create complex parts via different deposition techniques. To fabricate mechanically robust and stable structures using 3D printing with material properties well suited to the application, total control of droplet size, solidification rate, temperature gradients in the substrate and droplet, adhesion between the layers, and droplet impact velocity and direction are required. The complexity of the physics of 3D printing, involving cooling down from melting point of molten material, emerges from the intertwined effect of droplet impact dynamics and solidification [1]. As molten droplet being jetted and spreads on previous layer of same or different solidified material, a process involving spreading and solidification/remelting of contact line of a new layer, while substrate temperature as well as surface wettability have been found to play a role in ripple formation at periphery of splat [2]. To enhance the resolution and integrity of the printed parts, it is essential to have a thorough understanding of the physical phenomena involved so as to determine and control the maximum spread factor, $\varepsilon = R^*/R_0$ where R_0 is the pre-impact droplet radius, R^* is the maximum radius during spreading, as well as the relevant physical properties such as surface tension, σ, viscosity,μ, fluid density, ρ, thermal conductivity, k, etc [1–8].

Despite the wide range of experimental and numerical studies performed in this field, the physics of non-isothermal spreading and solidification arrest are still relatively unknown. Most of the work done in this field is based on solving the energy conservation equation between the pre-impact kinetics and interfacial energies and the final energy loss to viscous dissipation and surface deformation [9]. For example, one of the first analytical studies considering coupled fluid spreading and solidification of impinging metal droplets was done by Madejski [10]. In his attempt to find the maximum spread factor, he used the axisymmetric two-dimensional radial flow model with solidification emerging from the centerline and assumed that droplet forms a cylinder of radius R enlarging with time. His analytical model was based on the balance of the initial kinetic energy of the droplet and change in surface energy due to droplet deformation and work done in overcoming liquid viscosity during impact. In his calculations, he failed to include the effect of undercooling, surface wetting, and advancing contact angle, all of which lead to significant discrepancies between his theoretical model and experiments. Collings et al. [11] also studied the impact dynamics and solidification of liquid droplets analytically. One modification that they implemented in their analysis was considering the effect of contact angle. However, they made the assumptions that viscous dissipation and initial surface energy are negligible and the advancing and equilibrium contact angles are inseparable, so as a result, the obtained values from their analytical modeling did not bear out in experiments.

Watanabe et al. [12] employed a simple numerical simulation method neglecting the effect of viscous dissipation to predict the maximum droplet deformation and solidification progress on a cold target. They considered the fluid dynamics and phase change process to be uncoupled and occurring independently. In other words, they assumed that solidification occurs after the droplet deformation is complete regardless of the impact conditions and the temperature gradients. Pasandideh-Fard et al. [13] studied the impact of droplet on solid surface both experimentally and numerically.

Measured values of dynamic contact angle from experiment were used as boundary conditions for the numerical model. In order to find the effect of droplet solidification on the maximum spread diameter, they assumed that all kinetic energy stored in the solidified layer is lost.

The scope of the experimental work done on the evolution of the impacting drop base diameter during simultaneous spreading and solidification is quite limited. Most of the previous research is focused on bouncing and splashing effects of liquid droplets [14–17], and others remain limited to isothermal spreading [18, 19] which is fundamentally different from the solidifying dynamic contact-line problem as solidification plays a crucial role in controlling the molten contact line arrest. Schiaffino and Sonin [20, 21] performed an experimental study of the behavior of a deforming contact line as the flow spreads and solidifies on a sub-cooled target. They realized that, prior to arrest, the relationship between the dynamic contact angle and contact-line speed appears to obey the Tanner-Hoffman law [22, 23] assuming the equilibrium contact angle is zero. However, their study was limited to non-isothermal spreading of liquid over the solid of the same material and had approximately the same thermal properties. Their assumptions were not supported experimentally including (1) the solidification initiates from the basal plane at the trijunction and (2) the droplet would stop spreading when the contact angle at the solidification front reaches the dynamic contact angle of spreading. Bhola and Chandra [24] performed an experimental study on molten wax droplet impact. Aziz et al. [25] studied the impact and solidification of molten metal droplets experimentally under different initial impact velocity and target temperatures. They also used the energy balance criterion to assess the maximum spread factor for metal droplets. Their focus was to study the spray coating process and to find a prediction for the number of fingers created by the impact of molten droplets, and more importantly, they were only interested in metal droplets with high contact angles. More recently, Koldeweij et al [26] utilized total internal reflection to study the arrest of spreading sessile droplets. They hypothesized that crystal growth rate predicted the pinning of the contact line. Their work represent a lesser degree of subcooling than other works but may present a new mode of contact line arrest. A similar work by Herbaut et al. [27] made a similar observation where the growth of the dendritic structure caught the triple line and pinned it. Similar to the work by Koldeweij this is a much lower degree of subcooling and may represent a different form of contact line arrest.

Tavakoli et al. [28] performed an experimental and theoretical study on the dynamics of spreading drops on undercooled glass substrate. They proposed a new hypothesis to explain the arrest of solidification layer during spreading. They believed that the droplet stops spreading when the volume of the solidified region reaches a critical value. Their hypothesis is based on the initiation of solidification at the contact line and its progression through the liquid following the isotherms. They were able to show that the spread factor is proportional to $Ste^{-1/3}$, where $Ste = C_p(T_m - T_w)/L_f$, and C_p, T_m, T_w, and L_f are the specific heat, the melting temperature of the liquid, the temperature of a solid substrate, and the latent heat of fusion of the liquid, respectively. Higher Stefan number indicates a lower substrate temperature, or more significant subcooling. Tavakoli showed this relation for low velocity deposition of droplets using scaling analysis and verify their results with experiments; however, their analytical results

Table 1 The previous studies on different regimes of impact velocities for droplet spreading on solid substrate followed by solidification

$We \ll 1$	$We \sim 1$	$We \gg 1$
Schiaffino et al. [20]		Bennett et al. [38]
Clanet et al. [36]	Bhola et al. [24]	Aziz et al. [25]
Tavakoli et al. [28]	This work	Dhiman et al. [39]
Ruiter et al. [37]		Thiévenaz et al. [40]

are justified mathematically with unexplained mechanism involving critical volume. Meanwhile, their work is limited to low velocity, forced spreading.

Therefore, the models of droplet impact and solidification to this date either have not been validated by experimental results or cannot adequately explain the physics behind the non-isothermal spreading. Furthermore, the majority of the analytical studies are based on solving the energy balance equation, which is not sufficient for describing the motion and dynamics of impinging droplets [29]. It should also be noted that the prior works in this field focus on either low impact velocity deposition where the impact dynamics are negligible or the very high impact velocities in the splashing regime, both of which are extremely hard to control and predict. This study focuses on filling the gap between the very low and very high impact velocities, a region which is referred to as the moderate impact velocities in Table 1. In this work, we aim to examine the coupled solidification and spreading for a droplet of impact velocity in the intermediate region where the deposition velocities are still high but no splashing is observed and explain the process both analytically and experimentally. The ultimate goal of this paper is to fully control and predict the final shape of the droplet and maximum spread factor in order to maximize the resolution and efficiency of 3D printers.

We present, here, a new hypothesis explaining the arrest of spreading droplets of moderate impact velocities, and a set of experiments to verify the validity of this hypothesis. Based on our analysis, for a droplet impinging on a sub-cooled surface at moderate velocities, the final spreading diameter is determined by liquid and surface properties and is independent of impact velocity and degree of sub-cooling. First, we start by analyzing the governing equations for flow in this regime and obtain the final diameter of spreading based on the proposed hypothesis. The analytical modeling is followed by a series of experiments for different alkanes with properties listed in Table 2, all of which show great agreement with the model predictions. The details of the analytical model and experiments are presented in the following section.

2 Formulation and estimates

Figure 1 shows the droplet configuration before and during droplet spreading and solidification on a flat plate. In our proposed mathematical model, it is assumed that droplet of initial diameter D_0 strikes a surface perpendicularly with the free fall impact velocity V_i. The fluid flow during droplet impact and spreading is formulated using the axisymmetric coordinate system. The liquid is assumed to be incompressible. The droplet is characterized by initial temperature T_i, density ρ, dynamic viscosity μ,

Table 2 Properties of the fluids at room temperature

Fluid	Density (kg/m^3)	Absolute viscosity (kg/m s)	Surface tension (mN/m)	Latent heat (J/kg)	Specific heat capacity (J/g K)	Thermal Conductivity (W/m K)	Melting point (°C)
n-Hexadecane	773	3.34×10^{-3}	29.23	2.29×10^5	2.31	0.21	18.6
n-Pentadecane	769	3.70×10^{-3}	25.90	2.05×10^5	2.23	0.17	9.9

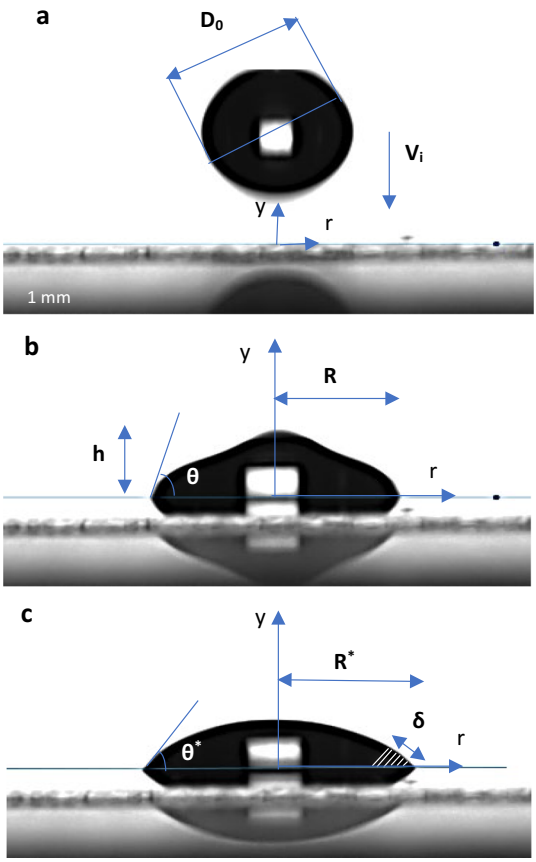

Fig. 1 Sequence of droplet deposition and spreading on a solid substrate of temperature lower than its melting point

thermal diffusivity α, and the substrate has a fixed temperature of T_w which is lower than the droplet melting temperature. Any effect from the ambient air on the droplet including the convective heat transfer is considered negligible. As the droplet hits the surface, it starts spreading in the r-direction; however, because of the temperature gradient near the substrate, liquid near the surface at the trijunction starts solidifying

as it spreads (dynamical contact angle < 90 degrees near onset of contact line arrest for most our experiments). As the liquid at the contact-line solidifies, the solidified region gets pinned to the surface and stops the spreading. The solidification onset mode can be either basal or lateral [30] depending on the droplet contact angle where 90° is the threshold value. Here, we focus on the motion and arrest of the contact line for fluids of contact angle less than 90° where solidification mode is lateral, suggesting the solidification front that induces a mechanism effective for contact line pinning initiates from the trijunction and freezing propagates inside the droplet perpendicular to the isotherms.

To determine the arrest diameter and quantify the effect of different initial conditions such as impact velocity, degree of substrate subcooling, fluid properties, on spreading of the droplet experiencing phase-change, we have performed scaling analysis of the governing equations. We start with the momentum equation at the contact line:

$$\left[\frac{\partial \overrightarrow{V}}{\partial t} + \left(\overrightarrow{V}.\nabla\right)\overrightarrow{V}\right] = -\frac{\nabla \mathrm{P}}{\rho} + \overrightarrow{\mathrm{g}} + \upsilon\nabla^2\overrightarrow{V} \tag{1}$$

Based on the scaling analysis of the continuity equation, it can be shown that $V \sim Uh/R$ where U and V are the velocity in the r and y directions, respectively. We plugged this result into the r-momentum equation combined with the assumption that $h/R \ll 1$, valid for wetting liquids. In the limit of moderate impact velocities, where spreading is driven by impact-induced forces but no fingering or instabilities occur at the trijunction, i.e. $We = \rho V^2 D/\sigma > 1$ and $Re = \rho V D/\mu > 1$, the flow at the contact line is driven by the impact and resisted via inertia and capillary pressure at the contact line. The upper limit of this regime can be established with the commonly used splash parameter $We\sqrt{Re} \leq 3000$ which corresponds to a Weber number of 114 for the n-hexadecane and 121 for the n-pentadecane used in this work [31]. Here, we have neglected the viscous effects on the grounds that at relatively low Ohnesorge number Oh, where $Oh = \mu/\sqrt{\rho\sigma D}$, the thickness of the boundary layer is very small compared to other flow dimensions; hence, the inviscid flow assumption [21]. For inviscid flow inside the droplet, $\frac{\upsilon U}{h^2}$ is comparably smaller than $\frac{\Delta P}{\rho R}$, so that the force balance at the contact line becomes:

$$\frac{U^2}{R} \sim \frac{\Delta P}{\rho R} \tag{2}$$

At the free surface, the normal stresses are replaced by an equivalent surface pressure, calculated from the interface mechanical equilibrium condition given by Laplace's equation, $\Delta P = \sigma\kappa$, where σ is the liquid–gas surface tension, and κ is the interface mean curvature at the trijunction. This curvature can be easily estimated using the geometry of droplet, $\kappa = R_0/R^2$, where $R_0 = \frac{D_0}{2}$. Using these equations, we can simply and find the spreading radius as a function of time and fluid properties as follows:

$$R \sim \sqrt[4]{\frac{\sigma R_0}{\rho}} t^{\frac{1}{2}} \tag{3}$$

It should be noted that Eq. (3) corresponds to the inertial spreading, which is the initial stage of spreading after the droplet hits the substrate. For moderate impact velocities the onset of solidification, the solidified front growth, and its subsequent arrest happen during the kinematic spreading stage.

3 Theory and hypothesis

As the droplet is spreading over the surface, the liquid near the surface at the trijunction begins solidifying. Prior to the onset of solidification, the droplet spreading mirrors the isothermal spreading dynamics regardless of the degree of undercooling. As the liquid starts solidifying and solidification front grows, it pins the contact line to the surface and halts the spreading. The solidification front grows in time following the well-known solidification equation [32], $\delta = \sqrt{4\alpha t Ste}$. It should be noted that since the size of the droplets is small, no nucleation consideration is necessary [33, 34]. There are different hypotheses regarding the contact-line pinning due to solidification, all with limited successes.

Our hypothesis for solidification arrest is that as the mass of solid is enlarging, the friction force increases (the friction force is proportional to the mass of the solidified region), and eventually, the friction force will reach the static friction force, f_s, which stops the movement of the contact line and spreading of droplet on the surface (Fig. 2). In other words, the arrest of contact line in non-isothermal spreading occurs due to the increase in the friction force applied to the solidified material, which further stops the spreading of the liquid behind it. To entertain this hypothesis, we have studied the force balance at the solidified region:

$$\frac{d}{dt}(m_s U) = \mu m_s g \tag{4}$$

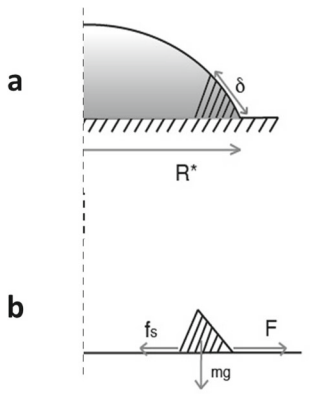

Fig. 2 **a** The axisymmetric view of the growth of solidification front following the isotherms for a droplet on a surface with contact angle smaller than 90°. **b** The force balance on the solidified region

$$m_s = \pi R \rho_s \delta^2 tan\theta \tag{5}$$

where R,θ, ρ_s, and μ are spreading radius and contact angle, density of solidified material, and friction coefficient. Equation (4) is the force balance for the solidified material. The solidified material is growing and moving at the contact line as a result of droplet spreading, while the friction between the solidified material and substrate is resisting this motion. Equation (6) is the result of applying the order of magnitude analysis to Eq. (4), which shows the balance of inertia and friction force for the solidified region.

$$\frac{U}{t} \sim \mu g \tag{6}$$

Taking the scaling analysis one step further, the contact-line velocity in r-direction is scaled by the ratio of spreading radius divided by time of spreading as shown in Eq. (7).

$$\frac{R}{t^2} \sim \mu g \tag{7}$$

Finally, combining the previously derived equation for spreading dynamics, Eq. (3), with Eq. (7), the time factor is eliminated.

$$\frac{\sigma R_0}{\rho R^3} \sim \mu g \tag{8}$$

Based on our hypothesis, the spreading stops when the friction force reaches its maximum value, the static friction, characterized by maximum coefficient of friction, μ_{max}. Thus, to find an order magnitude estimate for the final arrest radius, R^*, the friction coefficient is replaced by maximum coefficient of friction, $\mu_{\max} = 0.15$ as described in previous work [35] which results in the following:

$$\frac{\sigma R_0}{\rho R^{*3}} \sim \mu_{\max} g \tag{9}$$

By rearranging Eq. (9), we can then obtain Eqs. (10) and (11), which shows the arrest radius and spread factor, respectively, for the droplet impinging onto a solid substrate with moderate impact velocity. It should be noted that based on these results, the arrest radius is independent of impact velocity and/or the degree of undercooling, and it only depends on solid and fluid physical properties as well as the initial volume of the droplet.

$$R^* \sim \sqrt[3]{\frac{\sigma}{\rho \mu_{max} g}} \sqrt[3]{R_0} \tag{10}$$

$$\varepsilon \sim \sqrt[3]{\frac{\sigma}{\rho \mu_{\max} g R_0^2}} \tag{11}$$

To verify the results of the analytical modeling, experimental measurements for two different liquids of similar properties and same initial volume are performed over a variety of dynamic and thermal conditions. The predicted value for ε based on the materials is found to be approximately 3.

4 Experimental results and discussion

Experiments are carried out inside Krüss DSA 100 at various combinations of the substrate temperature, droplet impact velocity, dispensing needle position, and dispensing flow rate. Krüss DSA100 is also used for recording the droplet spreading dynamics and subsequent data evaluation. In principle, the Krüss DSA 100 machine consists of three main components (i) the specimen table with three manual knobs for accurate 3D positioning (ii) the video system with CCD camera, prism, light source and aperture (iii) a software-controlled multiple substance dosing unit. This state-of-the-art apparatus provides accurate measurement of the dynamic contact angle and base diameter of the spreading fluid. The intelligent dosing system of Krüss DSA 100 allows liquid to be dispensed without the risk of contaminating the sample. The bright light with extremely low radiated heat provides us with the illumination required for measuring drop radius evolution. The drop is illuminated from one side and a camera at the opposite side records images of the drop spreading and solidification. Temperature of the solid targets can be adjusted by a Peltier element situated in Krüss DSA100 machine from − 30 °C to 160 °C.

The free fall impact experiments of single drops are conducted for a range of *We* from 1 to 95 which corresponds to *Re* ranging from 62 to 637 and *Ste* from 0.1 to 0.3 on glass slides with dimensions of $50 \times 24 \times 0.15\ \text{mm}^3$ (VWR microcover glass). The substrate is rinsed successively in acetone, methanol, and DI water. Different impact velocities are obtained by changing the height of the needle with respect to the solid target. Higher elevations of the injection needle correspond to higher Weber numbers. During the liquid discharge from the injection needle, the drop becomes larger in size and eventually falls under its own weight. The volume of droplet is set to 5 μl and kept constant for all the experiments. In all experiments, the arrested base radius, R^* is measured at the moment that the spreading drop gets pinned due to solidification initiation.

In these experiments n-Hexadecane and n-Pentadecane are used as test fluids. The fluid characteristics are listed in Table 2. The reported values for the fluid properties are provided by the manufacturer. The contact angle values, both equilibrium and advancing, are measured for each set of experiments, and all the values were found to be consistently below 90°, which is the criterion for the analytical modeling. Impacting speeds and non-dimensional parameters of impact *We* and substrate Ste are tabulated in Table 3.

Figure 3 shows a comparison between the isothermal and non-isothermal spreading under the same impact conditions. It can clearly be seen how solidification pins the spreading contact line to the surface, and changes the profile and final shape of the solidified droplet. Based on the experimental data presented in Figs. 4, 5, and 6, as the impact velocity increases, the arrest radius becomes entirely independent of *Ste*

Table 3 Droplet impact speeds and non-dimensional parameters in experiments

Impact speed V [m/s]	*We* (n-Hexadecane)	*We* (n-Pentadecane)	*Ste*
0.14	1.10	1.23	0.124
0.84	39.6	44.5	0.161
0.90	45.1	50.6	0.182
0.95	50.6	56.8	0.202
1.05	61.6	69.2	0.222
1.14	72.6	81.5	0.242
1.22	83.6	93.9	0.262
1.30	94.6	106.6	0.283

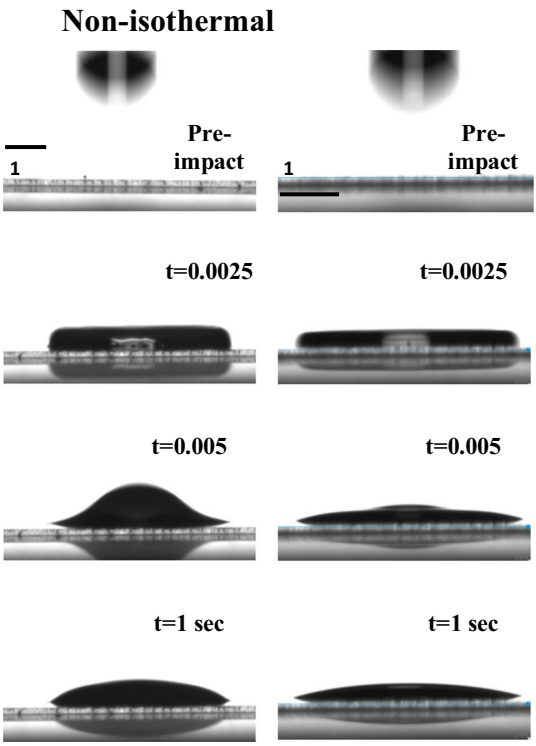

Fig. 3 The video sequence of the impact and spreading of an n-Hexadecane droplet on with and without solidification. The drop has the initial volume of 5 μl. The comparison of non-isothermal and isothermal spreading of impinging drops under the same impact dynamics shows the effect of lateral solidification on the arrest of contact line. The substrate temperatures for non-isothermal and isothermal experiment are − 20 °C and 20 °C, respectively

and *We,* which is aligned with the prediction of our analytical model. Figure 4 shows the spread factor versus *Ste* for different impact velocities of a n-Hexadecane droplet on a glass substrate. Each point on this plot is the average of five sets of experiments. It is clear that for low *We* experiments (*We = 1.10*), the radius of droplet is changing rapidly with *Ste;* however, as *We* increases and the droplet impact velocity falls within the moderate velocity regime, the plot becomes a plateau, and the arrest radius becomes

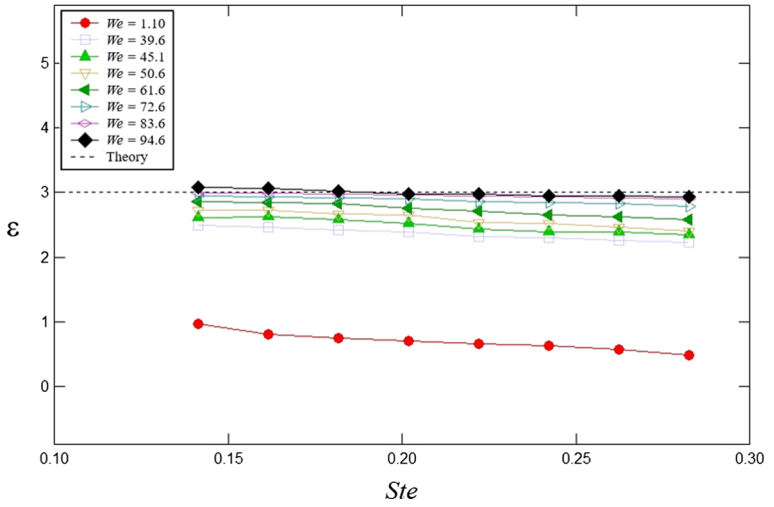

Fig. 4 Spread factor as a function of *Ste* for free fall of n-Hexadecane on glass substrates. The values of impact velocities corresponding to different *We* are the following: 0.14, 0.84, 0.90, 0.95, 1.05, 1.14, 1.22, and 1.30 m/s

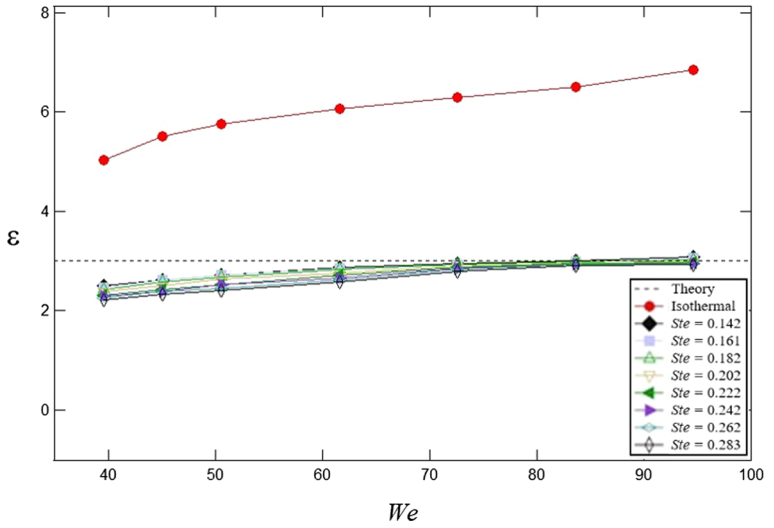

Fig. 5 Spread factor as a function of *We* for free fall of n-Hexadecane on glass substrates at moderate impact velocities with and without solidification

independent of both *Ste* and *We*. Figure 5 shows the results for droplets of moderate impact velocities with and without solidification. For sub-cooled substrates it is shown that as *We* increases, all the lines merge into one single value for one spread factor of the droplet. This outcome is consistent with the prediction of our analytical model (dashed line on Figs. 4, 5, and 6) and prior experimental data. Certain discrepancy

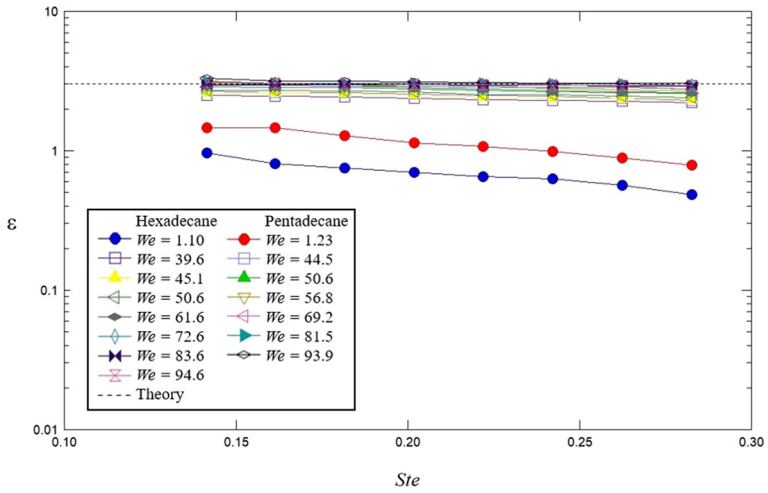

Fig. 6 Spread factor as a function of *Ste* for free fall of n-Pentadecane and n-Hexadecane on glass substrates. The dashed lines on all figures represent the predicted value by the analytical model which is in good agreement with the experimental results. The values of impact velocities for both fluids are the following: 0.14, 0.84, 0.90, 0.95, 1.05, 1.14, 1.22, and 1.30 m/s

between model and experiment may be resulted from the fact that the scaling does not include the onset of freezing at contact line to create freezing-induced friction and that the estimation of $\mu_{\max}$ at contact line may differ from its actual value in experiments. However, the concise model provides an asymptotic prediction while neglecting complexity in modeling, matching reasonably well with the experiment. For the isothermal spreading on the other hand, the final radius is clearly increasing with increasing impact velocities and is much higher than the final radius of spreading coupled with solidification, all of which highlight the importance of solidification on controlling the spreading dynamics in the moderate regime.

As both n-Hexadecane and n-Pentadecane droplets have similar properties and initial volume, the measure of arrest radius should be approximately the same based on the proposed hypothesis. To test our hypothesis further, same sets of experiments are performed using n-Pentadecane and the results are plotted and superimposed with n-Hexadecane data in Fig. 6. For low *We* experiments of both fluids, it is shown that arrest radius is decreasing as *Ste* increases and the measured values of arrest radius for n-Pentadecane are considerably different in comparison to the n-Hexadecane. However, at moderate impact velocity experiments, the spread factor becomes approximately the same and in great agreement with the predicted value from the analytical model.

5 Conclusion

To summarize, we have performed an experimental and theoretical study on the dynamics of non-isothermal spreading of impinging droplets with moderate impact velocities.

In this range of velocities, the impact velocities are high enough that the impact-induced forces play an important role in droplet spreading and cannot be neglected, but the velocities are low enough to ensure fingering instabilities and/or break-ups do not occur.

A new hypothesis is presented, aiming to explain the physics behind the spreading dynamics attenuated by solidification. This hypothesis is based on the initiation of the solidified layer from the contact line and ascending through the liquid bulk. *We* have shown that as the mass of the solid is growing due to solidification while the measure of kinetic friction also grows the same rate and, eventually, the kinetic friction reaches the value of static friction which stops the movement of the contact line. The scaling analysis suggests that in the case of moderate impact velocity deposition of droplets, the arrest radius of the drop only depends on fluid and surface properties and initial volume of droplet and is independent of initial impact velocity and temperature difference between the solid substrate and droplet.

To verify the analytical results, a series of experiments are performed using different liquids under a variety of initial conditions. The values of arrest radius for moderate velocities are measured using a high-speed photography. The results show that the R^* for moderate impact velocity experiments (no fingering or breakup instabilities) and small arrested contact angles (less than 90°) is independent of *We*, *Ste*, and other initial conditions. Therefore, the effect of solidification on the spreading dynamics in this region is very important as it limits the spreading to a certain arrest radius that cannot be altered by merely changing the impact velocities and/or temperature gradients.

Thus, there exists a stable non-isothermal spreading regime independent of initial conditions, which allows us to entirely control and adjust the footprint which is applicable to many areas of industry for such as additive manufacturing and inkjet printing.

Author contributions H.P.K. proposed and supervised the work. R.M. and E.A. designed experiments and built the experimental setup. R.M. and E.A. performed experiments. R.M. and E.A. analyzed and explained data. R.M., E.A., and H.P.K. interpreted and discussed the results. S.D. advised on the approach at early stages. R.M., E.A., and H.P.K. prepared the figures. R.M., E.A., P.Y., and H.P.K. wrote the main manuscript text. R.M., E.A., P.Y., and H.P.K. reviewed the manuscript.

Data availability The data that support the findings of this study are available from the corresponding author upon reasonable request.

Declarations

Conflict of interest The authors declare no competing interests.

References

1. Lohse D (2022) Fundamental fluid dynamics challenges in inkjet printing. Annu Rev Fluid Mech 54(1):349–382
2. Gilani N, Aboulkhair NT, Simonelli M, East M, Ashcroft IA, Hague RJM (2022) From impact to solidification in drop-on-demand metal additive manufacturing using MetalJet. Addit Manuf 55:102827
3. Attinger D, Poulikakos D (2001) Melting and resolidification of a substrate caused by molten micro-droplet impact. J Heat Transfer 123(6):1110–1122

4. Haferl S, Butty V, Poulikakos D, Giannakouros J, Boomsma K, Megaridis CM, Nayagam V (2001) Freezing dynamics of molten solder droplets impacting onto flat substrates in reduced gravity. Int J Heat Mass Transf 44(18):3513–3528
5. Haferl S, Poulikakos D (2003) Experimental investigation of the transient impact fluid dynamics and solidification of a molten microdroplet pile-up. Int J Heat Mass Transf 46(3):535–550
6. Li Ri, Ashgriz N, Chandra S (2010) Maximum spread of droplet on solid surface: low Reynolds and Weber numbers. J Fluids Eng 132:061302
7. Luo J, Qi LH, Zhong SY, Zhou JM, Li HJ (2012) Printing solder droplets for micro devices packages using pneumatic drop-on-demand (DOD) technique. J Mater Process Technol 212(10):2066–2073
8. Bot Le, Cédric SV, Arquis E (2005) Impact and solidification of indium droplets on a cold substrate. Int J Therm Sci 44(3):219-233.3
9. Chandra S, Avedisian CT (1991) On the collision of a droplet with a solid surface. Proc R Soc Lond A 432(1884):13–41
10. Madejski J (1976) Solidification of droplets on a cold surface. Int J Heat Mass Transf 19(9):1009–1013
11. Collings EW, Markworth AJ, McCoy JK, Saunders JH (1990) Splat-quench solidification of freely falling liquid-metal drops by impact on a planar substrate. J Mater Sci 25:3677–3682
12. Watanabe T, Kuribayashi I, Honda T, Kanzawa A (1992) Deformation and solidification of a droplet on a cold substrate. Chem Eng Sci 47(12):3059–3065
13. Pasandideh-Fard M, Chandra S, Mostaghimi J (2002) A three-dimensional model of droplet impact and solidification. Int J Heat Mass Transf 45(11):2229–2242
14. Engel OG (1955) Waterdrop collisions with solid surfaces. J Res Natl Bur Stand 54(5):281–298
15. Levin Z, Hobbs PV (1971) Splashing of water drops on solid and wetted surfaces: hydrodynamics and charge separation. Philos Trans R Soc London Ser A Math Phys Sci 269(1200):555–585
16. Loeher KF, Lasek A (1990) Splashing of drops arch. Mech Warszawa 42: 6
17. Rein M (1993) Phenomena of liquid drop impact on solid and liquid surfaces. Fluid Dyn Res 12(2):61–93
18. Ford DM, Elliott TA (1974) Dynamic contact angles. Part 8—impact spreading of water drops in air and aqueous solutions of surface active agents in vapour on rough paraffin wax surfaces. J Chem Soc Faraday Trans 1 Phys Chem Condens Phases 70:423–430
19. Stow CD, Hadfield MG (1981) An experimental investigation of fluid flow resulting from the impact of a water drop with an unyielding dry surface. Proc R Soc London A Math Phys Sci 373(1755):419–441
20. Schiaffino S, Sonin AA (1997) Molten droplet deposition and solidification at low Weber numbers. Phys Fluids 9(11):3172–3187
21. Schiaffino S, Sonin AA (1997) Motion and arrest of a molten contact line on a cold surface: an experimental study. Phys Fluids 9(8):2217–2226
22. Tanner LH (1979) The spreading of silicone oil drops on horizontal surfaces. J Phys D Appl Phys 12(9):1473
23. Hoffman RL (1975) A study of the advancing interface. I. Interface shape in liquid—gas systems. J Colloid Interface Sci 50(2):228–241
24. Bhola R, Chandra S (1999) Parameters controlling solidification of molten wax droplets falling on a solid surface. J Mater Sci 34:4883–4894
25. Aziz SD, Chandra S (2000) Impact, recoil and splashing of molten metal droplets. Int J Heat Mass Transf 43(16):2841–2857
26. Koldeweij RBJ, Kant P, Harth K, de Ruiter R, Gelderblom H, Snoeijer JH, Lohse D, van Limbeek MAJ (2021) Initial solidification dynamics of spreading droplets. Phys Rev Fluids 6(12):L121601
27. Herbaut R, Brunet P, Limat L, Royon L (2019) Liquid spreading on cold surfaces: Solidification-induced stick-slip dynamics. Phys Rev Fluids 4:033603
28. Tavakoli F, Davis SH, Pirouz Kavehpour H (2014) Spreading and arrest of a molten liquid on cold substrates. Langmuir 30(34):10151–10155
29. Bejan A, Gobin D (2006) Constructal theory of droplet impact geometry. Int J Heat Mass Transf 49(15–16):2412–2419
30. Alizadeh-Birjandi E, Pirouz Kavehpour H (2017) Plant leaves icephobicity. J Coat Technol Res 14:1061–1067
31. Josserand C, Thoroddsen ST (2016) Drop impact on a solid surface. Annu Rev Fluid Mech 48:365–391
32. Stefan J (1889) Über einige probleme der theorie der wärmeleitung. Sitzungber Wien Akad Mat Natur 98:473–484
33. Clyne TW (1984) Numerical treatment of rapid solidification. Metall Trans B 15:369–381

34. Dykhuizen RC (1994) Review of impact and solidification of molten thermal spray droplets. J Therm Spray Technol 3:351–361
35. Kavehpour HP, McKinley GH (2004) Tribo-rheometry: from gap-dependent rheology to tribology. Tribol Lett 17:327–335
36. Clanet C, Béguin C, Richard D, Quéré D (2004) Maximal deformation of an impacting drop. J Fluid Mech 517:199–208
37. Ruiter De, Rielle PC, Brunet P, Snoeijer JH, Gelderblom H (2017) Contact line arrest in solidifying spreading drops. Phys Rev Fluids 2(4):043602
38. Bennett T, Poulikakos D (1993) Splat-quench solidification: estimating the maximum spreading of a droplet impacting a solid surface. J Mater Sci 28:963–970
39. Dhiman R, Chandra S (2005) Freezing-induced splashing during impact of molten metal droplets with high Weber numbers. Int J Heat Mass Transfer 48(25–26):5625-5638.8
40. Thiévenaz V, Séon T, Josserand C (2019) Solidification dynamics of an impacted drop. J Fluid Mech 874:756–773